Journal of the Taiwan Institute of Chemical Engineers 108 (2020) 29–42

Contents lists available at ScienceDirect

Journal of the Taiwan Institute of Chemical Engineers

journal homepage: www.elsevier.com/locate/jtice

Full cycle dynamic optimisation maintaining the operation margin of acetylene hydrogenation fixed-bed reactor

Fu-Ming Xie, Feng Xu*, Zhi-Shan Liang, Xiong-Lin Luo

Department of Automation, China University of Petroleum Beijing, 102249, China

ARTICLE INFO

Article History:
Received 19 September 2019
Revised 17 December 2019
Accepted 18 January 2020
Available online 5 February 2020

Keywords:
Process engineering systems
Dynamic optimisation
Operation margin
Control vector parameterisation
Acetylene hydrogenation reactor

ABSTRACT

In an acetylene hydrogenation reactor, the slowly falling catalyst activity affects ethylene plant performance in an operating cycle. To maximize the integral economic benefit in a regeneration cycle or achieve the longest regeneration cycle, the full cycle operation optimisation must be a long time-scale dynamic optimisation for which the method of control vector parameterization is adopted. Because of various uncertain disturbances, some distances must be reserved for process constraints and the desired effect of full cycle optimisation is hardly fully achieved. Thus, based on the strictly slowly-time-varying catalyst deactivation model, the operation margin consumption is estimated. Furthermore, a modified full cycle operation optimisation strategy is presented which takes the operation margin consumption as additional constraints. To obtain the maximum integral economic benefit or the longest regeneration cycle, we present a realizable full cycle optimized operation plan that considers the sufficient operation space reserved for uncertain disturbances.

1. Introduction

1.1. Literature review

Acetylene hydrogenation reactors are used to convert acetylene in high concentration ethylene stream. Acetylene hydrogenation reactor is a complex nonlinear system, which can be described by two modelling approaches the pseudo-homogeneous and heterogeneous model. For simplified modelling, one-dimensional pseudo-homogeneous model has been widely accepted [9,40,41]. Acetylene hydrogenation reactors extensively utilise improved bimetallic catalyst and the pseudo-homogeneous model is also built [12,26]. The accuracy of heterogeneous model is higher than that of pseudo-homogeneous model, but the heterogeneous model suffers from high computation complexity [18,36].

Since the catalyst activity is usually decreasing slowly with time, a catalyst deactivation model should be built [1,17,20,30,31]. Several catalyst deactivation models of acetylene hydrogenation reactors have been proposed, which mainly considered that the decreasing catalyst activity is related to the temperature and poisoning effect [4]. In practical processes, the fitted curves from industrial data are often adopted for catalyst deactivation modelling, which is of no universality. Hence, the deactivation kinetics model based on two-dimensional heterogeneous model has been proposed, and the optimal economic benefits could be obtained by operation optimisation, which only considers the steady-state operation (the objective function is diurnal economic benefit) and did not consider margin consumption [42].

To improve industrial competitiveness, operation optimisation provides a unified framework for reducing production costs, meeting safety requirements and environmental regulations, improving product quality, and reducing product variability. In most chemical processes, operation optimisation is always treated as steady-state optimisation. But for a slowly-time-varying process such as acetylene hydrogenation reactor, it should be treated as a long time-scale dynamic process. Thus, the full cycle operation optimisation must be a dynamic optimisation. Dynamic optimisation is commonly used in aerospace system [29], electric [22] and petrochemical process systems [10,35]. Considering the complexity and uncertainty, the dynamic optimisation of chemical process cannot be solved easily. As an application of dynamic optimisation, acetylene hydrogenation process is discussed from the optimisation model to the solving methods [38,39]. In petrochemical process, only the numerical method can be used to solve the dynamic optimisation problem. Considering the model complexity, the method of control vector parameterisation (CVP) is widely used for solving the dynamic optimisation problem, where the control vector is parameterised by finite parameters in each time interval [23,27]. CVP has been discussed in detail by many scholars [3,5,6,11,37]. However, in the actual process, because of various uncertain disturbances, some distances must be reserved for process constraints and the desired effect of full cycle optimisation is hardly fully achieved [19,43].

Because of the slow-time-varying characteristic, with the changes of slowly-time-varying parameters, the operating point slowly deviates from the steady-state optimum design point. The performance of chemical plant will become worse, even some process constraints may be violated. Moreover, various uncertain disturbances may also perturb the operating point from the desired steady-state optimum design point.

* Corresponding author.
E-mail addresses: xufeng@cup.edu.cn, xufengfxzt@sohu.com (F. Xu).

https://doi.org/10.1016/j.jtice.2020.01.008
1876-1070/

Nomenclature

Parameters

a	specific surface area of catalyst(m^{-1})
τ	number of axial discretization in the reactor
ω	number of radial discretization in the reactor
ω_1	frequency of disturbance
σ	catalyst porosity
η_1, η_2	efficient factor of the ethylene and ethane generated reaction
λ_R^s, λ_R^g	the catalyst and the gas phase heat conductivity coefficient of reactor radial direction ($W\ m^{-1}\ K^{-1}$)
c_p	heat capacity ($J\ kg^{-1}\ K^{-1}$)
D_{Ra}, D_{Rb}, D_{Rc}	acetylene, ethylene and hydrogen diffusion coefficient of reactor radial ($m^2\ s^{-1}$)
E_1, E_2, E_3	activation energy of reaction coefficients of the ethylene, ethane and green oil generated reaction ($J{\cdot}mol^{-1}$)
E_d	activation energy of catalyst deactivation ($kJ\ kmol^{-1}$)
ΔH_1, ΔH_2	heat of the ethylene and ethane generated reaction ($J\ mol^{-1}$)
h_w	interphase heat transfer coefficient ($W\ m^{-1}\ K^{-1}$)
k_1, k_2, k_3	reaction coefficients reaction coefficients of the ethylene, ethane and green oil generated reaction
k_d, K_d	catalyst deactivation coefficients
K_p	proportional gain of PID controller
K_I	integration time of PID controller
K_D	differentiation time of PID controller
M_a, M_b, M_c	acetylene, ethylene and hydrogen price coefficient ($RMB\ kPa^{-1}\ day^{-1}$)
R_g	gas constant ($J\ mol^{-1}\ K^{-1}$)
t_2, t_3	step change and one-order inertia link time constant of disturbance
v_1,v_2,v_3	sine wave, step change, and one-order inertia link amplitude of disturbance

Variables

θ	catalyst activity
ε	broadened constraint
ρ	average density ($kg\ m^{-3}$)
δ_j^E,δ_j^R	The conversion factors of bounds in model 7 and 8
ω_1	time of slowly-time-varying system(day)
Γ_f	maximum operating period(day)
C_g	Green oil concentration (mole fraction)
$\boldsymbol{d}$	the optimal design variables
$\mathbf{\Delta d}$	process margin
$\Delta \boldsymbol{d}_c$	control margin
Ea,Eb,Ec	the function of acetylene, ethylene and hydrogen economic benefits
$\boldsymbol{e}$	steady state error
ΔF	The upper limits of economic benefits
ΔF_1	The upper limits of diurnal catalyst activity decreased
$\boldsymbol{f}$	equality constraint of the slowly-time-varying system
$\boldsymbol{g}$	inequality constraints of the slowly-time-varying system
Δg_j^E,Δg_j^R	sum of surplus and control margins solved using model 3 and 6
$\boldsymbol{h}$	dynamic state equations of the fast-time-varying system
$\boldsymbol{h_s}$	steady state equations of the fast-time-varying system
N	time interval of CVP
p_a, p_b, p_c	acetylene, ethylene and hydrogen pressure in the reactor (kPa)
p^s, p^g	the catalyst and the gas phase average gas pressure in the reactor (kPa)
p_{i1}, p_{i2}, p_{i3}	gas pressure in the 1−3 stage reactor(kPa)
R	dimensionless radius of the reactor
r_a, r_b, r_c	reaction rate of acetylene, ethylene and hydrogen in the reactor ($mol\ m^{-3}\ s^{-1}$)
r_g	reaction rate of green oil in the reactor ($mol\ m^{-3}\ s^{-1}$)
r_1, r_2, r_3	reaction rate in the 1−3 stage reactor ($mol\ m^{-3}\ s^{-1}$)
T^s, T^g	the catalyst phase and the gas phase temperature in the reactor (K)
T_1, T_2, T_3	temperature in the 1−3 stage reactor(K)
t	time of fast-time-varying system(minute)
$\boldsymbol{U}$	control variable
$\boldsymbol{u}$	optimisation variable
x	dynamic state variables of the fast-time-varying system
$\bar{x}$	steady state variables of the fast-time-varying system
Z	dimensionless axial of the reactor

For this problem, sufficient margins must be added for design variables to allow sufficient distances between the operating point and process constraints and prevent process variables from breaking process constraints after slowly-time-varying parameters become "worse". The current research on margin mainly focused on enhancing the operation flexibility of chemical plants involving controllability evaluation [16], dynamic economic analysis [34], resiliency index [13] and design margin [32]. The chemical process is designed to ensure safe operation and product quality. However, the design margins are usually determined according to the worst-case influence of various uncertainties, while the changes of slowly-time-varying parameters from the initial state to the "worst" state is a slowly dynamic process. Many researchers have proposed simultaneous process and control integration design methods for heat exchanger network and fluid catalytic cracking unit, which can ensure the satisfaction for process performance under the various uncertainties [19,43].

To coordinate the control and optimisation problems under the uncertain disturbances, a "back-off" method for estimating the influence of uncertain disturbances is proposed, and the distance between operating points and constrain boundaries is defined [24,25]. The "back-off" method is early applied to improve the steady state optimisation effect for dynamic processes [2,7]. Furthermore, the optimisation of complex nonlinear models is enabled using "back-off" method [15,21,28]. The stochastic simulation using a given probability distribution is used by "back-off" method, improving the computational efficiency [8,33]. In recent years, the "back-off" method has been applied to the optimisation method of integrated design, optimisation and control [14]. For a slowly-time-varying system, the "back-off" method can offset the effect of uncertainties. However, it still needs to combine certain effect of the slowly-time-varying parameters, when coordinating the control and optimisation problems.

1.2. Our contributions

The systematic calculation of operation optimisation relies on the precise mathematical models. Particularly during the long period of

the full cycle operation optimisation using complex nonlinear models, a small deviation caused by the initial modelling error can greatly affect the entire operation during operating cycle. In this paper, a mechanistic modelling approach is used based on acetylene hydrogenation intrinsic kinetics and catalyst deactivation kinetics. During the operation optimisation of an acetylene hydrogenation reactor, the equivalent catalyst activity is generally assumed in all internal sites of the reactor for most of research [9,12,18,26,36,40,41]. However, in this paper, considering the integrity of the acetylene hydrogenation reactor and the complexity of dynamic running, the internal catalyst activity is handled as distributed parameter. The acetylene hydrogenation reactor is expected to be operated for the maximum integral economic benefit in certain regeneration cycle or the longest regeneration cycle, whose outlet acetylene concentration is the main constraint of operation optimisation. Sometimes, for maintaining the long-time steady operation of the ethylene plant, the longer regeneration cycle is more preferred than economic benefit. The full cycle operation optimisation is solved via the CVP method on a long time-scale. Considering that the time scale of full cycle operation dynamic optimisation is in days and the time scale of process controllers is in minutes or seconds, the model of acetylene hydrogenation reactor and its control system are running on short time-scale whereas the full cycle operation optimisation is solved on a long time-scale. However, if the full cycle operation optimisation and the control system are both carried out on a unified platform, it can cause computational complexity. Thus, the two systems should run on different platforms and some variables of them are shared.

The design margins are determined by the worst-case influence of various uncertainties, and must make up the influence of slowly-time-varying parameters and uncertain disturbances. Thus, one part of margin consumption is a long time-scale dynamic process affected by slowly-time-varying parameters, at the same time, another part of margin consumption is serving for control system to resist the uncertain disturbances under short time-scale. In our study, considering the dynamic processes of the slowly-time-varying parameters and the uncertain disturbances under different time scales, the consumed margins involving process margins (for slowly-time-varying parameters) and control margins (for operation and control) in an operation cycle are estimated through on-line optimisation.

The maximum potential benefit from operation optimisation is determined by the distances between the current operating point and process constraints, which is related to the operation margins of design variables. Considering the various disturbances in chemical processes, some distances must be reserved for fluctuations of process variables. Thus, the operation optimisation must not fully explore the operation space from design margins. The maximum potential benefit is related to the design margins minus the consumed process margins, while the achievable benefit is related to the design margins minus the consumed process and control margins. In our study, the economic benefits of operation optimisation (including the maximum potential benefit and achievable benefit) are estimated on-line according to the distances between the operating point and active constraints. Furthermore, a modified full cycle operation optimisation strategy is presented which takes the operation margin consumption as additional constraints. A full cycle optimized operation plan maintaining sufficient operation space can be obtained.

2. Modelling and structure of full cycle operation dynamic optimisation

2.1. Preliminary work

As a representative slowly-time-varying process, with the effect of slowly-time-varying parameter (catalyst activity), the acetylene hydrogenation reactor is expected to be operated for longer regeneration cycle or more economic benefit at the same time satisfying the product quality requirements. Compared with other uncertainties in process, the decreasing of catalyst activity is inevitable but predictable, and it has a significant effect on product [18]. Thus, the modelling of acetylene hydrogenation reactor focuses on catalyst deactivation modelling based on the intrinsic kinetics. Catalyst activity decreasing is a complex process involving the surface temperature variation of catalyst, the accumulated oligomer of secondary reaction and the change in molecular structure [38]. For catalyst activity, the greatest short-run influence is from the temperature variation of the catalyst surface. Nonetheless, the long-run influence is from the clogging of the surface micro-pores by the accumulated oligomer of the secondary reaction product (green oil) leading to slowly catalyst deactivation.

The catalyst activity θ is defined as a distributed parameter related to the radial and axial direction distance, that is $\theta(Z, R)$. Corresponding to the catalyst activity of an arbitrary point in the reactor, the oligomer concentration is also defined as a distributed parameter related to the radial and axial direction distance, that is $C_g(Z,R)$. On the basis of the oligomer concentration of arbitrary point in the reactor, the kinetic equation of slowly catalyst deactivation is derived. Primarily, based on energy conservation and intrinsic kinetics, the following reaction rate equation of oligomer (green oil) producing is obtained [42]:

$$\frac{\partial C_g(Z,R,t)}{\partial t} = \frac{k_d {p^s_{ak}}^2(Z,R,t) p^s_{ck}(Z,R,t)}{\left(1 + K_d p^s_{ak}(Z,R,t)\right)^3} \tag{1}$$

p is the gas partial pressure in the reactor. Subscripts a, b, c represent acetylene, ethylene and hydrogen respectively. Subscript k denotes the sequence number of reactor bed with $k = 1, 2, 3$. Superscripts s and g represent the variable of gaseous and solid phase equation for the heterogeneous model.

For the equation of green oil concentration, two sides of Eq. (1) are integrated over t. Furthermore, the temperature is considered as the key factor for increasing adjustability of catalyst activity. Based on thermal deactivation kinetics, the reaction rate equation of catalyst deactivation is represented as Eq. (2), where T is temperature in the reactor [42].

$$\frac{\partial \theta_k(Z,R,t)}{\partial t} = -k_d e^{\left(-\frac{E_d}{R_g T^s_k(Z,R,t)}\right)} C_g(Z,R,t) \tag{2}$$

Then, by substituting the equation of C_g (green oil concentration) into Eq. (2), the following reaction rate equation of catalyst deactivation is obtained:

$$\frac{\partial \theta_k(Z,R,t)}{\partial t} = -k_d e^{\left(-\frac{E_d}{R_g T^s_k(Z,R,t)}\right)} \int_0^t \frac{{p^s_{ak}}^2(Z,R,\zeta) p^s_{ck}(Z,R,\zeta)}{\left(1 + K_d p^s_{ak}(Z,R,\zeta)\right)^3} \mathrm{d}\zeta \tag{3}$$

2.2. Structure of full cycle operation optimisation

The process-based model for the three stages of reactor bed is the foundation for full cycle operation optimisation. We substitute the Eq. (3) into the heterogeneous model of the acetylene hydrogenation reactor to obtain a stricter and more suitable model, whose detailed description is shown in the Appendix A.

The simulation of fast-time-varying system and the optimisation of slowly-time-varying system based on mechanism models are implemented simultaneously. In a fast-time-varying system, PID controllers should be used to compensate for the bad affection of uncertain disturbances. We design the control systems in which the temperature and hydrogen inlets of the three stage reactors are the manipulated variables of six PID controllers. The PID controller parameters are shown in Table 1.

To ensure the simultaneous operation of slowly-time-varying system and the fast-time-varying system, we propose the following structure of simulation implementation on double platforms at the

Table 1
Parameters of the controllers.

Operation variable		Proportional gain	Integral time	Derivative time
Temperature inlets	First stage reactor	0.6	6	
	Second stage reactor	0.6	7	
	Third stage reactor	0.5	7	
Hydrogen inlets	First stage reactor	30	8	0.1
	Second stage reactor	30	7	0.1
	Third stage reactor	30	5	0.1

same time. The long time-scale unit of slowly-time-varying system in days is represented by Γ. To obtain the catalyst activity of the Γ day, the reaction rate of catalyst deactivation is integrated, as shown in Eq. (4).

$$\theta_k(Z,R,\Gamma)=\theta_k(Z,R,0) -\int_0^{\Gamma} k_d e^{\left(\frac{E_d}{R_g T_k^s(Z,R,t)}\right)} \int_0^t \frac{{p_{ak}^s}^2(Z,R,\zeta)p_{ck}^s(Z,R,\zeta)}{\left(1+p_{ak}^s(Z,R,\zeta)\right)^3}\mathrm{d}\zeta\mathrm{d}\psi \tag{4}$$

However, considering the computation complexity, we ignore the short time-scale dynamic fluctuation of process variables in one day. Thus, we take the mean values of process variables in one day into Eq. (4), and Eq. (4) is transformed into a discrete form as Eq. (5).

$$\theta_k(Z,R,\Gamma)=\theta_k(Z,R,0) -\sum_{i=1}^{\Gamma} k_d e^{\left(\frac{E_d}{R_g T_k^s(Z,R,i)}\right)} \sum_{j=1}^{i} \frac{{p_{ak}^s}^2(Z,R,j)p_{ck}^s(Z,R,j)}{\left(1+p_{ak}^s(Z,R,j)\right)^3} \tag{5}$$

The structure of simulation implementation is shown in Fig. 1. The optimised operation variable $\boldsymbol{u}$ is sent to the fast-time-varying system, which maintains the normal running of the reactor through the PID controllers. Correspondingly, when the fast-time-varying system is running on steady state through the PID controller, the steady state variables represented as $\bar{\mathbf{x}}$ are transferred to the slowly-time-varying system. In addition, during the on-line margin estimation, the state variable of the fast-time-varying system are transferred to the on-line margin estimator to calculate the surplus margins. Then, the optimised variables that ensure a certain operation margin are obtained using the optimiser. Simulation software gPROMS is used to build the model and control system, and the optimizer is built on MATLAB software.

3. Full cycle operation optimisation of acetylene hydrogen reactor

For acetylene hydrogenation reactors, we want more economical benefit and longer regeneration cycle while ensuring the quality of outlet ethylene product. With longer regeneration cycle of catalyst, the inlet hydrogen can be increased and the inlet temperature for activity compensation can be reduced but leading to increased economic consumption. Our operation optimisation will coordinate the incompatibility between the two problems. The full cycle operation optimisation is a long time-scale dynamic optimisation whose time unit is day.

Generally speaking, there are two main types of method for solving dynamic optimisation, namely numerical method and analytical method. However, efficiently obtaining a high-quality solution for such dynamic optimisation is challenging and difficult. Especially when the problem contains large-scale models, solving the Hamiltonian for complex processes is almost impossible through analytical methods when the calculus of variations is used. By time discretization, the numerical method transforms the infinite dimensional dynamic optimisation problem to finite dimensional nonlinear programming problem [3,5,6,11,23,27,37]. Although an optimal solution for the Pontryagin's maximum principle cannot be obtained, the numerical method is simple and easy be solved, which is widely used in the chemical processes. The model of acetylene hydrogenation reactor is considered as a high non-linear complex model. Hence, the dynamic optimisation problem is only solved using numerical methods. In addition, to simplify the calculation of dynamic optimisation, the distributed parameter system should transform the original distributed parameter system into an equivalent large-scale lumped system. Through radial and axial discretisation, the numbers of the radial and axial interval are represented by ω and τ, respectively, as shown in Eq. (6). Hence, the dynamic optimisation model easier to be solved is obtained.

$$\begin{cases} [0,Z]\rightarrow[0,Z_1), & [Z_1,Z_2), & \cdots, & [Z_{\lambda-1},Z_\lambda), & \cdots, & [Z_{\omega-1},Z_\omega) \\ [0,R]\rightarrow[0,R_1), & [R_1,R_2), & \cdots, & [R_{\lambda-1},R_\lambda), & \cdots, & [R_{\omega-1},R_\omega) \end{cases} \tag{6}$$

In addition, considering both the simulation implementations of fast-time-varying and slowly-time-varying systems, Γ_f is defined as the cycle of catalyst regeneration, and short time-scale state variables and long-time-scale state variables $\mathbf{x}, \bar{\mathbf{x}}$ are represented as follows:

$$\begin{aligned} \boldsymbol{x} &= \left[\mathbf{x}_1, \quad \mathbf{x}_2, \quad \cdots, \quad \mathbf{x}_\Gamma, \quad \cdots, \mathbf{x}_{\Gamma_f}\right] \\ \bar{\boldsymbol{x}} &= \left[\bar{\mathbf{x}}_1, \quad \bar{\mathbf{x}}_2, \quad \cdots, \quad \bar{\mathbf{x}}_\Gamma, \quad \cdots, \bar{\mathbf{x}}_{\Gamma_f}\right] \end{aligned} \tag{7}$$

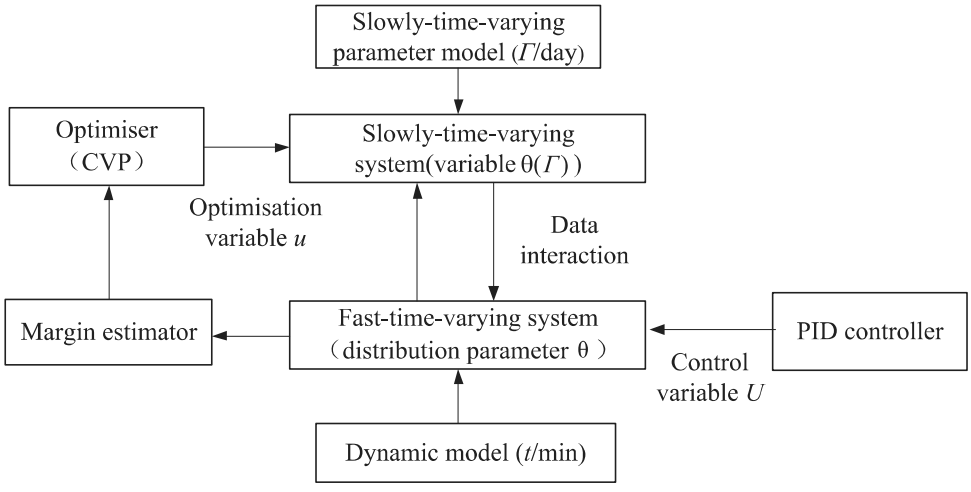

Fig. 1. Structure of slowly-time-varying system.

The CVP method divides the time duration of the whole dynamic process into several time intervals. The optimisation horizon is divided into several time intervals, which are shown in Eq. (8).

$$[0,\Gamma_f] \to [0,\Gamma_1),\quad [\Gamma_1,\Gamma_2),\quad \cdots,\quad [\Gamma_{\lambda-1},\Gamma_\lambda)\quad \cdots,\quad [\Gamma_{N-1},\Gamma_N) \tag{8}$$

N is the number of time intervals which determines discrete precision. The discrete optimisation variable is shown in Eq. (9).

$$\boldsymbol{u}(\Gamma) = [u_1(\Gamma_1),\quad u_2(\Gamma_2),\quad \cdots,\quad u_\lambda(\Gamma_\lambda),\quad \cdots,\quad u_N(\Gamma_N)] \tag{9}$$

$u_\lambda(\Gamma_\lambda)$ represents the trajectory of $u(\Gamma)$ in $[\Gamma_{\lambda-1},\quad \Gamma_\lambda)$, whose value is invariable for piecewise constant strategy. For the fast-time-varying system in a full cycle, the equations of process-based model and control system model for the acetylene hydrogen reactor in Table 1 are represented as $\boldsymbol{h}(\blacksquare)$, as shown in Eq. (10).

$$\mathrm{h}(\mathrm{x},\mathrm{u},t) = \left[h_1(\mathrm{x}_1,u_1,t), h_2(\mathrm{x}_2,u_1,t),\cdots,\mathrm{h}_\Gamma(\mathrm{x}_\Gamma,\mathrm{u}_\lambda,\mathrm{t}),\cdots,\mathrm{h}_{\Gamma_f}(\mathrm{x}_{\Gamma_f},\mathrm{u}_N,\mathrm{t})\right]^{\mathrm{T}} \tag{10}$$

By CVP, the optimisation variables are converted into a set of parameters, that is, the original dynamic optimisation problem is transformed into the finite dimensional nonlinear programming problem. The nonlinear programming problem an approximation of the original dynamic optimisation problem, and their difference is eliminated while N tends to be infinite, but increasing N increases the computation.

3.1. Operation optimisation for economic benefit

In this section, we implement the full cycle operation optimisation to maximise the integral economic benefit in certain regeneration cycle. For constructing the function of ethylene economic benefits in the Γ day, the radial average ethylene partial pressure of the end stage reactor outlet is multiplied by the ethylene price coefficient $\mathrm{M_b}$, as shown in Eq. (11).

$$E_\mathrm{b}(\Gamma) = \frac{\mathrm{M_b}}{\tau}\sum_{R=0}^{R_\tau} p^\mathrm{s}_{\mathrm{b}3}(1,R,\Gamma) \tag{11}$$

Similarly, by calculating the summation of the hydrogen and acetylene pressure difference between the inlet and outlet of the reactor, the economic benefit consumption in Γ day is obtained, as shown in Eq. (12).

$$\begin{aligned} E_\mathrm{a}(\Gamma) &= \frac{\mathrm{M_a}}{\tau}\sum_{R=0}^{R_\tau}\sum_{k=1}^{3}\left(p^\mathrm{s}_{ak}(1,R,\Gamma) - p^\mathrm{s}_{ak}(0,R,\Gamma)\right) \\ E_\mathrm{c}(\Gamma) &= \frac{\mathrm{M_c}}{\tau}\sum_{R=0}^{R_\tau}\sum_{k=1}^{3}\left(p^\mathrm{s}_{ck}(1,R,\Gamma) - p^\mathrm{s}_{ck}(0,R,\Gamma)\right) \end{aligned} \tag{12}$$

The economic benefit of the full-cycle is obtained by integrating the diurnal economic benefits, which are the economic benefit differentials of reactant gases, as shown in Eq. (13).

$$J_1 = -\int_0^{\Gamma_f}\left(E_\mathrm{b}(\Gamma) - E_\mathrm{a}(\Gamma) - E_\mathrm{c}(\Gamma)\right)\mathrm{d}\Gamma \tag{13}$$

The inlet hydrogen partial pressures and inlet temperatures of three reactor stages are chosen as independent variables of dynamic optimisation, and the dynamic optimisation model is represented as follows:

Model 1

$$\min \quad J_1$$

$$\text{s.t.} \quad \boldsymbol{f}(\bar{\boldsymbol{x}},\boldsymbol{u},\Gamma) = 0$$

$$\boldsymbol{h}(\boldsymbol{x},\boldsymbol{u},t) = 0$$

$$\boldsymbol{g}(\bar{\boldsymbol{x}},\boldsymbol{u},\Gamma) \le 0$$

In the above model, $\boldsymbol{f}(\blacksquare)$ represents the catalyst deactivation model in the slowly-time-varying system and $\boldsymbol{g}(\blacksquare)$ represents the constraints of dynamic optimisation, including the operation horizons of the three stages of the acetylene hydrogen reactor and outlet acetylene concentrations of the end stage. The constraints of the full cycle operation optimisation include the initial and trajectory constraints as shown in Table 2. Relative to initial constraints, trajectory constraints are continually broadened for long-run decreasing catalyst activity effect. Broadened constraint $\boldsymbol{\varepsilon}$ depends on the reaction rate of decreasing catalyst activity and the control process of the fast-time-varying system. In addition, there is a necessary constraint for process requirements that the acetylene fraction of total gases of reactor outlet is lower than 5×10^{-6}.

Table 2
Constraints of the full cycle operation optimisation.

Operation variable		Initial constraint	Trajectory constraint
Temperature Inlets (K)	$T^\mathrm{s}_1(0,R,\Gamma_\lambda)$	[320,325]	$[T^\mathrm{s}_1(0,R,\Gamma_{\lambda-1})-\varepsilon_1, T^\mathrm{s}_1(0,R,\Gamma_{\lambda-1})+\varepsilon_1]$
	$T^\mathrm{s}_2(0,R,\Gamma_\lambda)$	[320,325]	$[T^\mathrm{s}_2(0,R,\Gamma_{\lambda-1})-\varepsilon_2, T^\mathrm{s}_2(0,R,\Gamma_{\lambda-1})+\varepsilon_2]$
	$T^\mathrm{s}_3(0,R,\Gamma_\lambda)$	[321.5,322.5]	$[T^\mathrm{s}_3(0,R,\Gamma_{\lambda-1})-\varepsilon_3, T^\mathrm{s}_3(0,R,\Gamma_{\lambda-1})+\varepsilon_3]$
Hydrogen Inlets (kPa)	$p^\mathrm{s}_{c1}(0,R,\Gamma_\lambda)$	[28.5,29.2]	$[p^\mathrm{s}_{c1}(0,R,\Gamma_{\lambda-1})-\varepsilon_4, p^\mathrm{s}_{c1}(0,R,\Gamma_{\lambda-1})+\varepsilon_4]$
	$p^\mathrm{s}_{c2}(0,R,\Gamma_\lambda)$	[13.8,14.2]	$[p^\mathrm{s}_{c2}(0,R,\Gamma_{\lambda-1})-\varepsilon_5, p^\mathrm{s}_{c2}(0,R,\Gamma_{\lambda-1})+\varepsilon_5]$
	$p^\mathrm{s}_{c3}(0,R,\Gamma_\lambda)$	[0.77,0.81]	$[p^\mathrm{s}_{c3}(0,R,\Gamma_{\lambda-1})-\varepsilon_6, p^\mathrm{s}_{c2}(0,R,\Gamma_{\lambda-1})+\varepsilon_6]$

The optimiser uses CVP to transform the original full cycle operation optimisation problem into a nonlinear programming problem, which can be solved using the sequential quadratic programming (SQP) method. However, considering the variations in the operating conditions due to the full cycle trajectories determined by the optimisation framework, the tuning PID parameters under specific conditions have to perform well under the full cycle trajectory. Therefore, it is necessary to optimize the PID parameters of the controller. Admittedly, the PID parameters of 6 controllers can be substituted into the optimisation framework as optimisation variables, but this method greatly increases the computational burden of the full cycle operation optimisation. Therefore, we propose a method to obtain the suboptimal solution using an iterative method. The steps are as follows:

(1) Solve model 1 under PID parameters are shown in Table 1;
(2) Fix the obtained optimisation variables and optimize the PID parameters in model 1;
(3) Fix the PID parameters obtained from optimisation of 2 and then solve model 1;
(4) Repeat steps 2 and 3 until the obtained PID parameters and optimisation variables are no longer changed.

The optimized PID parameter trajectories are shown in Fig. 2.

The results of the full cycle operation optimisation are shown in Table 3, and the optimal operation trajectory is shown in Fig. 3(a). The economic benefits of one year are obtained by solving the optimisation model. In addition, considering that the acetylene fraction in the total outlet gases is a hard constraint which cannot be violated, the regeneration cycle without optimisation is only 76 days, and economic benefit of no optimisation is only 2.78×10^5¥. No optimisation refers to the normal operation results of acetylene hydrogenation reactor under normal conditions. Reactor operation data under normal conditions are shown in Appendix C. For economic benefits and regeneration cycles, the results of dynamic optimisation whose objective is the maximum integral economic benefit in certain regeneration cycle are obviously superior to the results without optimisation.

The number of time intervals is a critical parameter in full cycle operation optimisation based on the CVP method. The obtained economic benefits with a different number of time intervals are arranged based on size order as $N = 10 < 18 < 30$, as shown in Table 3. Notably, the deviation between the obtained economic benefits of $N = 18$ and $N = 30$ is less than approximately 1.5%. Considering the computation complexity and optimisation accuracy, the suitable number of time intervals is approximately $N = 20-30$.

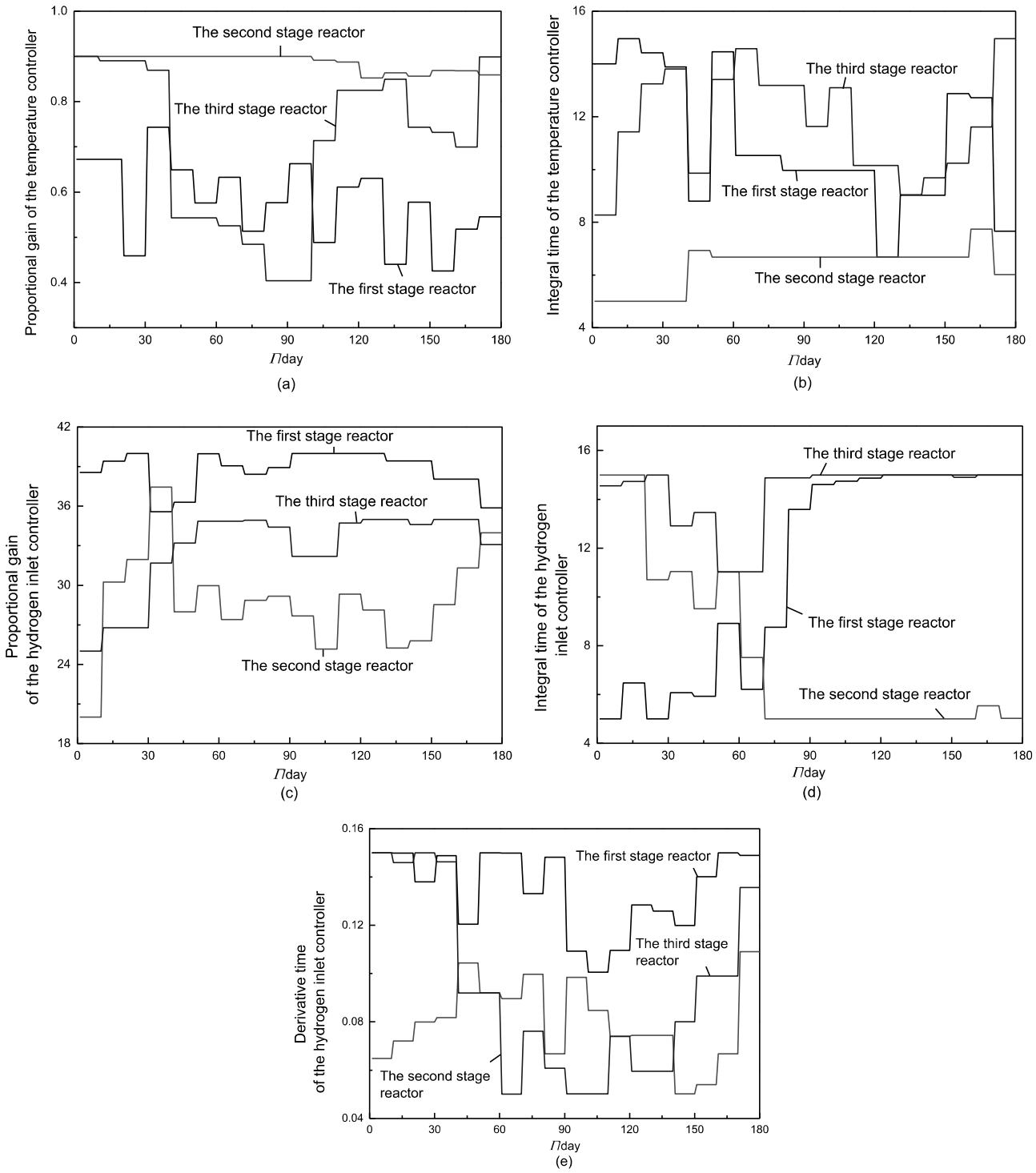

Fig. 2. Optimal curve of PID parameters.

Table 3
Parameters and results of the full cycle operation optimisation.

Optimisation parameters and results	Value		
The number of time interval (N)	10	18	30
Economic benefit of full cycle optimisation (¥/a)	1.43×10^6	1.55×10^6	1.57×10^6
Economic benefit of no optimisation (¥/a)	2.78×10^5	2.78×10^5	2.78×10^5

3.2. Operation optimisation for regeneration cycle

In coordination with the other operation requirement in the ethylene industry, the economic benefit is sometimes considered the secondary optimisation objective compared with regeneration cycle. The system influenced by slowly-time-varying parameters is stopped for catalyst regeneration when it reaches the regeneration cycle Γ_f. Therefore, the full cycle operation optimisation model whose objective is the longest regeneration cycle is represented as follows:

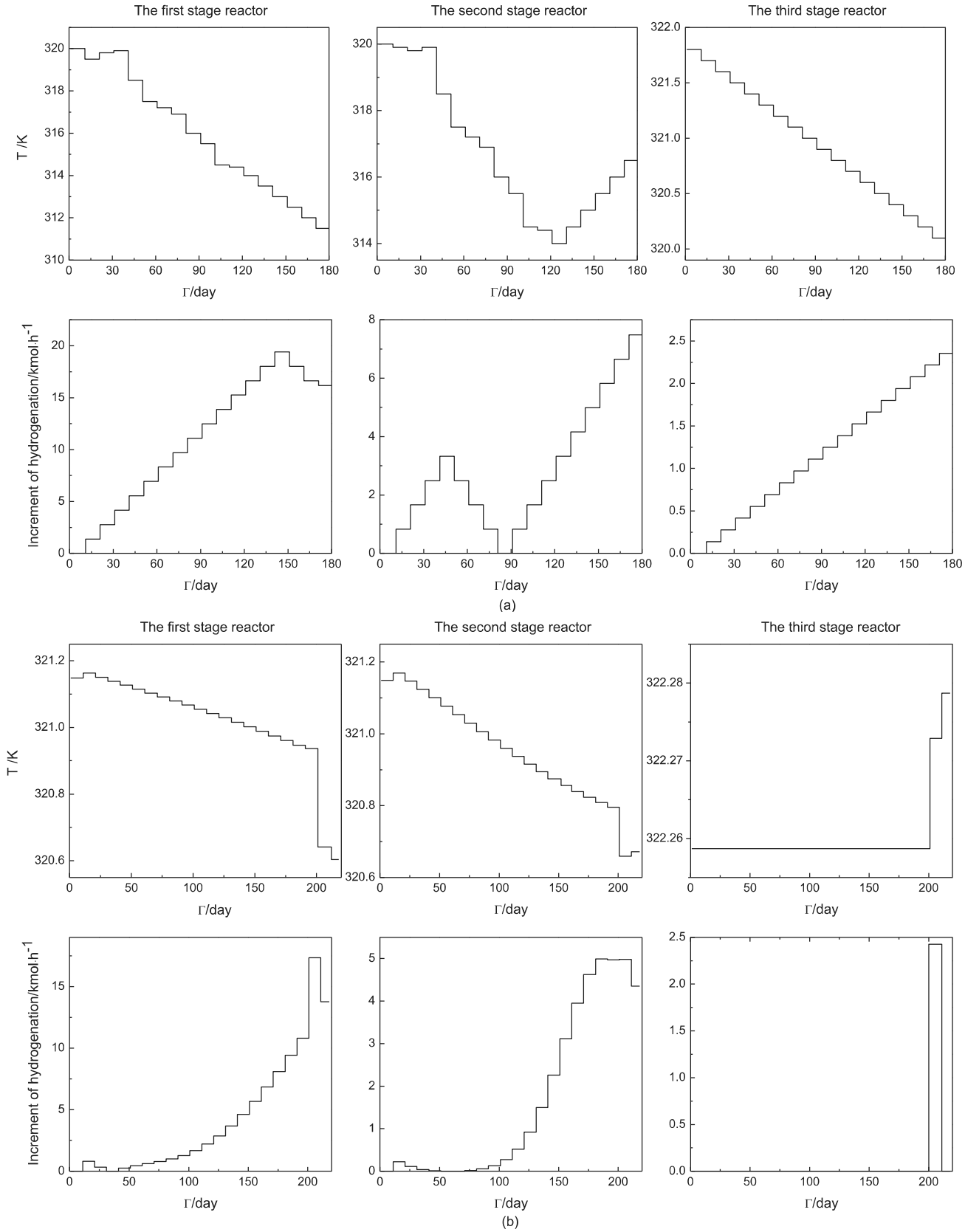

Fig. 3. Operation trajectory of full cycle optimisation: a) Operation trajectory of solved model 1; b) Operation trajectory of solved model 2.

Model 2

$$\min \quad J_2 = -\Gamma_f$$

$$\text{s.t.} \quad \boldsymbol{f}(\bar{\boldsymbol{x}}, \boldsymbol{u}, \Gamma) = 0$$

$$\boldsymbol{h}(\boldsymbol{x}, \boldsymbol{u}, t) = 0$$

$$\boldsymbol{g}(\bar{\boldsymbol{x}}, \boldsymbol{u}, \Gamma) \leq 0$$

In the above model, Γ_f is defined as an integer variable, we should solve a mixed-integer dynamic optimisation problem. However, considering that there is one integer variable Γ_f, this mixed-integer dynamic optimisation problem can be simplified. To solve the mixed-integer dynamic optimisation problem, we can treat the integer variable Γ_f as a continuous variable to transform the problem into a continuous dynamic optimisation problem.

The optimal operation trajectory is shown in Fig. 3(b), and the curve of economic benefit is shown in Fig. 7. For the obtaining optimal regeneration cycle, we must suffer from a certain loss of economic benefits in the late operation phase. Hence, the optimal solution of the model 2 is 218.74 days, although the economic benefits obtained are less than those obtained with model 1.

In comparison with model 1, the operation trajectory of model 2 is smoother for maintaining catalyst activity. The temperature operation strategies of the two optimisation models are generally decreased for reducing the reaction rate of intrinsic activity deactivation. Correspondingly, the hydrogen inlet operation strategies of the two optimisation models generally increase for compensating economic loss with decreasing catalyst activity. In Fig. 3(a), considering that the catalyst activity in the first bed is close to the constraint boundary in the later period of regeneration cycle, the hydrogenation of the first bed decreases slightly to reduce the oligomer accumulation and maintain certain activity of the catalyst. It increases the acetylene at the inlet of the second bed, thus increasing the inlet temperature of the second bed of the reactor. In Fig. 3(b), the full cycle operation optimisation for the longest regeneration cycle chooses the strategy with slowly operating inlet temperature and inlet hydrogen. In comparison with the initial operating point, the maximum operation deviation of inlet temperature is less than ±1 K and the maximum operation deviation of the inlet hydrogen is less than 20 kmol h^{-1}. The catalyst activity of the first and second beds would become very low and the hydrogenation reaction is hardly running in the later period of the regeneration cycle. For extending the regeneration period, the third bed of the reactor should be used as far as possible to ensure the percentage of acetylene at the outlet. Therefore, the inlet temperature of the first and second beds of the reactor decreased obviously, and the inlet temperature and hydrogenation in the third bed increased. The simulation on the optimised strategies of model 1 can obtain more benefits but shorter regeneration cycle, while the other simulation on the optimised strategies of model 2 can maintain a longer regeneration cycle but less benefits. Exact optimisation plan should depend on practical production requirement.

4. Full cycle operation optimisation maintaining operation margin

The off-line dynamic optimisation strategy whose objective is the maximum integral economic benefit in certain regeneration cycle or the longest regeneration cycle can be used to determine an optimal solution for the ideal experiment. However, considering the various disturbances in chemical processes, some distances must be reserved for the fluctuations of process variables and that the optimum operating point is not on some process constraints. Accordingly, the design margin for reactor length must be added for sustained system operation throughout the regeneration cycle. Accordingly, a full cycle operation optimisation strategy that keeps operation margin and fully uses surplus margin is proposed.

4.1. Estimation of process and control margin

The margin is defined as the value added on the nominal value of the design variable because of process uncertainties. The total design margin consists of two parts: process margin and control margin. Process margin is designed for compensating the effect of the change in slowly-time-varying parameters, whereas control margin is designed for operation and control. During the design phase of chemical processes, sufficient margins must be added for design variables to ensure sufficient distances between the operating point and process constraints and prevent the process variables from breaking process constraints after slowly-time-varying parameters become “worse”. However, the design margins are usually determined according to the worst-case influence of various uncertainties, while the changes of slowly-time-varying parameters from the initial state to the “worst” state is a slowly dynamic process. Hence, the margin consumption is a long dynamic process affected by slowly-time-varying parameters and unmeasured parameters. As shown in Fig. 4, the process margin consumption is increasing with time, but control margin consumption fluctuates within a certain range. After the cycle, the surplus margin can be reduced to 0, and the sum of the process margin and the control margin is equal to the design margin.

To meet the constraints and for more economic benefit optimisation, the estimation of process margin and control margin is significant for slowly-time-varying chemical process. Process margin in Γ day can be obtained by solving the steady state optimisation model as shown in Model 3.

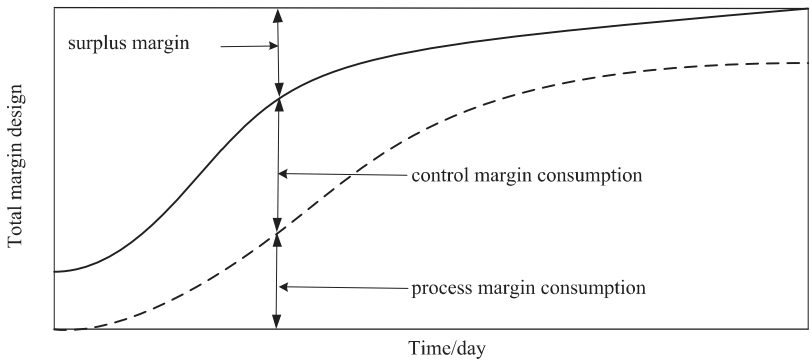

Fig. 4. Margin consumption.

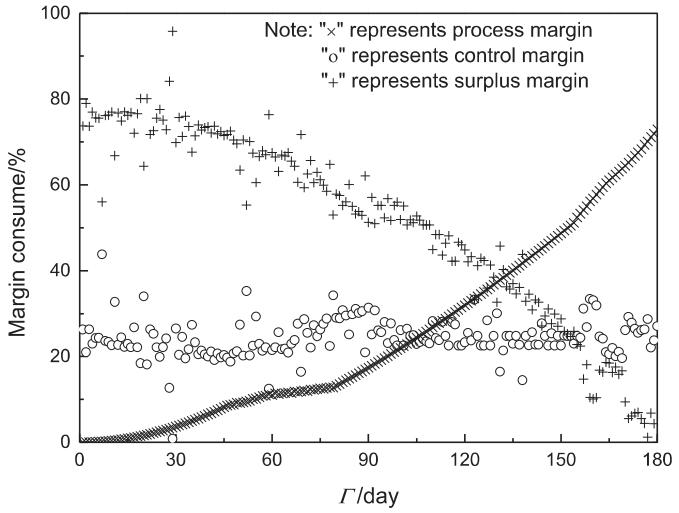

Fig. 5. Margin consumption at 180-day operation.

Model 3

$$\min_{u,d+\Delta d} \quad J_3 = -E_b(\Gamma) + E_a(\Gamma) + E_c(\Gamma)$$

$$\text{s.t.} \quad \boldsymbol{f}(\bar{\boldsymbol{x}}, \boldsymbol{u}, \Gamma) = 0$$

$$\boldsymbol{h}_s(\boldsymbol{x}, \boldsymbol{u}, t, \boldsymbol{d} + \Delta d) = 0$$

$$\boldsymbol{g}(\bar{\boldsymbol{x}}, \boldsymbol{u}, \Gamma, \boldsymbol{d} + \Delta d) \leq 0$$

$$\Delta d(\Gamma) \geq 0$$

In model 3, $\boldsymbol{d}$ represents the optimal design variables and $\mathbf{\Delta d}$ represents the process margin of optimal design variables. To facilitate the representation of control margin estimator, we transform the fast-time-varying dynamic system into quasi-steady-state equations as $\mathbf{h_s}$, which contain no control systems. During the actual process operation, with the variation of slowly-time-varying parameters, the process margin of the Γ day is represented as $\mathbf{\Delta d}(\Gamma)$. For complexity reduction, only the reactor length is treated as design variable in the acetylene hydrogenation reactor system. Then, to obtain the optimal design variables $\boldsymbol{d}$, we solved the steady state optimisation via model 4 for the economic benefits.

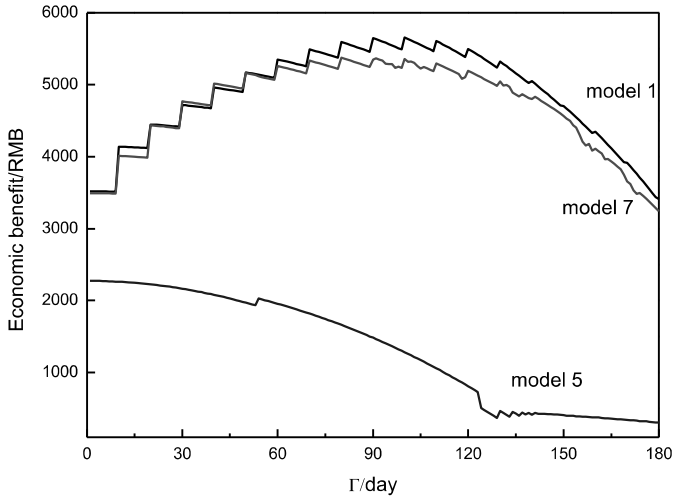

Fig. 6. Economic benefit curve of full cycle operation optimisation.

Model 4

$$\min_{u,d} \quad J_1$$

$$\text{s.t.} \quad \boldsymbol{f}(\bar{\boldsymbol{x}}, \boldsymbol{u}, \Gamma) = 0$$

$$\boldsymbol{h}_s(\boldsymbol{x}, \boldsymbol{u}, t, \boldsymbol{d}) = 0$$

$$\boldsymbol{g}(\bar{\boldsymbol{x}}, \boldsymbol{u}, \Gamma, \boldsymbol{d}) \leq 0$$

In addition, to satisfy operation and control the needs of long-term running, the control margin must be designed by solving the short time-scale dynamic optimisation model. The operation of control system must be considered to design the control margin. Hence, the dynamic equation of the PID control system is accounted in the short time-scale dynamic optimisation model, as shown in model 5.

Model 5

$$\min_{u,d+\Delta d+\Delta d_c} \quad J_3 = -E_b(\Gamma) + E_a(\Gamma) + E_c(\Gamma)$$

$$\text{s.t.} \quad \mathbf{f}(\bar{\mathbf{x}}, \mathbf{u}, \Gamma) = 0$$

$$\mathbf{h_s}(\mathbf{x}, \mathbf{U}, t, \mathbf{d} + \Delta d + \Delta \mathbf{d}_c) = 0$$

$$\mathbf{g}(\bar{\mathbf{x}}, \mathbf{u}, \Gamma, \mathbf{d} + \Delta d + \Delta \mathbf{d}_c) \leq 0$$

$$\boldsymbol{U}(t) = \mathrm{K}_P\left(\mathbf{e}(t) + \mathrm{K}_I^{-1}\int_0^t \mathbf{e}(t)dt + \mathrm{K}_D\frac{d\mathbf{e}(t)}{dt}\right)$$

$$\mathbf{e}(t) = \mathbf{u} - \mathbf{x}(t)$$

$$\Delta \boldsymbol{d}_c(\Gamma), \Delta \boldsymbol{d}(\Gamma) \geq 0$$

In model 5, $\mathbf{\Delta d}_c(\Gamma)$ represents the control margin of the optimal design variables in the Γ day. The solved result of the model 5 at the 180-day operation and the percentage of consumed process margin, consumed control margin and surplus margin in the total margin design are shown in Fig. 5.

The total design margin is defined as the summation of the process and control margin in the Γ_f day, represented as $\mathbf{d}(\Gamma_f) + \mathbf{\Delta d}(\Gamma_f) + \mathbf{\Delta d}_c(\Gamma_f)$. The percentage of process margin continuously increases until operation termination due to catalyst reactivation, and finally obtains approximately 80% of the total margin design. By contrast, the percentage of control margin fluctuates within approximately 20–30% of the total margin design. Exactly 80% of the total margin is remained at the reactor beginning and decreasing to 0 in the 180 day.

The benefit curve of the operation optimisation based on the above design margin is shown in Fig. 6. Although the total economic benefit is 4.75×10^5 ¥ and less than the results of model 1, the operation optimisation based on the margin saved can ensure that the system steadily runs even when faced with uncertain disturbances.

For estimating the process and control margin of the model whose object is the longer regeneration cycle, considering that the regeneration cycle is a full period variable, the minimum diurnal decreased activity is considered as object function to replace the regeneration cycle. In addition, to obtain diurnal decreased activity, the average of diurnal catalyst activity is extracted from the distributed parameter variable. The optimisation model is shown in model 6.

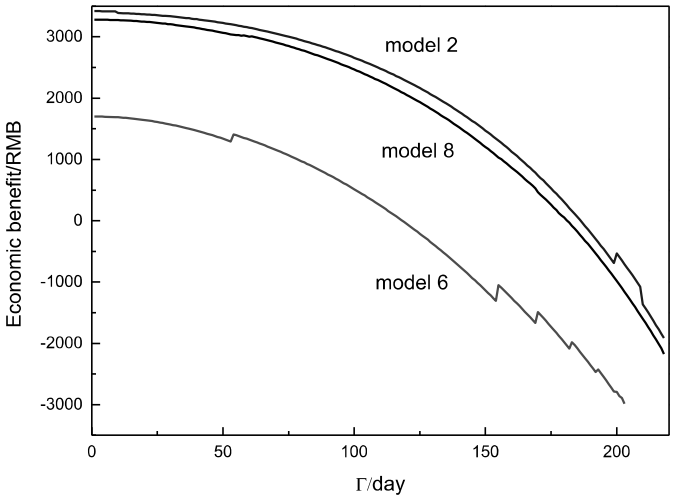

Fig. 7. Economic benefit curve of the full cycle operation optimisation for regeneration cycle.

Model 6

$$\min_{u,d+\Delta d+\Delta d_c} \quad J_4 = \frac{1}{\omega\tau}\left(\sum_{R=R_1}^{R_\tau}\sum_{Z=Z_1}^{Z_\omega}\theta(\Gamma-1,Z,R)-\sum_{R=R_1}^{R_\tau}\sum_{Z=Z_1}^{Z_\omega}\theta(\Gamma,Z,R)\right)$$

$$\text{s.t.} \quad \boldsymbol{f}(\bar{\boldsymbol{x}},\boldsymbol{u},\Gamma)=0$$

$$\boldsymbol{h_s}(\boldsymbol{x},\boldsymbol{U},t,\boldsymbol{d}+\Delta d+\Delta\boldsymbol{d}_c)=0$$

$$\boldsymbol{g}(\bar{\boldsymbol{x}},\boldsymbol{u},\Gamma,\boldsymbol{d}+\Delta d+\Delta\boldsymbol{d}_c)\leq 0$$

$$\boldsymbol{U}(t)=\mathrm{K}_P\left(\boldsymbol{e}(t)+\mathrm{K}_I^{-1}\int_0^t \boldsymbol{e}(t)dt+\mathrm{K}_D\frac{d\boldsymbol{e}(t)}{dt}\right)$$

$$\boldsymbol{e}(t)=\boldsymbol{u}-\boldsymbol{x}(t)$$

$$\Delta\boldsymbol{d}_c(\Gamma),\Delta\boldsymbol{d}(\Gamma)\geq 0$$

By solving model 6, the operation optimisation that ensures sufficient control margin is shown in Fig. 7, the economic benefit is less than that in model 2 and regeneration cycle is only 203 days.

4.2. Full cycle operation optimisation maintaining operation margin

The operation optimisation in Section 4.1 is based on the estimation of the design margin. However, the part of total design margin is not consumed until the maximum regeneration cycle. If the part of the design margin can be fully exploited, the full cycle operation optimisation can bring more economic benefits under the condition of ensuring sufficient margin. However, the part of the design margin cannot be immediately but instead slowly released with decreasing catalyst activity.

The Lagrange multiplier vector of inequality constraints $\mathbf{g}(\cdot)$ in models 3 and 6 of steady state optimisation is defined as $\boldsymbol{\mu}$, which contains active constraint $\mu_j \geq 0$ and non-active constraint $\mu_i = 0$. Base on the Kuhn–Tucker condition, the equations between active constraint and objective function are obtained. The Lagrangian function is shown in Eq. (14).

$$\begin{aligned}\Delta F &= -\sum \mu_j \Delta g_j^{\mathrm{E}} \\ \Delta F_1 &= -\sum \mu_j \Delta g_j^{\mathrm{R}}\end{aligned} \tag{14}$$

The steady state operating points of models 3 and 6 are on the boundary of active constraint; hence, $\boldsymbol{g}_j(\cdot)=0$, while process margin consumption exactly compensate for the influence of slowly-time-varying parameters. The sum of surplus and control margins solved using model 3 and 6 can move operating points inside the constraint, represented as $\Delta\mathbf{g}_j^{\mathrm{E}}, \Delta\mathbf{g}_j^{R} < 0$. The upper limits of economic benefits and diurnal decreased activity which are obtained by operation optimisation are equivalent to their declining quantity affected by surplus margin, represented as ΔF and ΔF_1.

Then, we can construct a function that describes the distance between operating points and constrained boundary, which is defined as the margin consumption function. The object function of model 1 is added by the margin consumption function for structuring the full cycle operation optimisation model which considers margin consumption, as shown in model 7.

Model 7

$$\min \quad J_5 = J_1 + \sum_j \delta_j^{\mathrm{E}} g_j^2(\cdot)$$

$$\text{s.t.} \quad \boldsymbol{f}(\bar{\boldsymbol{x}},\boldsymbol{u},\Gamma)=0$$

$$\boldsymbol{h}(\boldsymbol{x},\boldsymbol{u},t)=0$$

$$\boldsymbol{g}(\bar{\boldsymbol{x}},\boldsymbol{u},\Gamma)\leq 0$$

$$0 < \delta_j^{\mathrm{E}} g_j^2(\cdot) < \Delta F$$

The conversion factors of constraints are represented as δ_j^{E}; and the margin consumption function is represented as $\sum_j \delta_j^{\mathrm{E}} g_j^2(\cdot)$. Considering the optimisation results of model 5, we can estimate the control and process margin in the Γ day online. Then, we can calculate the economic benefit reduction caused by the influence of control and process margin. Their sum is equivalent to the minimum economic benefit loss in the Γ day, which is then substituted into model 7 to be solved for the full cycle operation optimisation problem. The solved results are shown in Table 4, and the economic benefits of 1.49×10^6 ¥ are obtained by full cycle operation optimisation maintaining operation margin. In comparison with the results of the full cycle operation optimisation without margin maintaining, considering the saved necessary control margin, the economic benefits of full cycle operation optimisation maintaining operation margin are less than that of the full cycle operation optimisation without margin maintaining. The economic benefit curve of reactor with respect to time is shown in Fig. 6.

For ensuring sufficient control margin for operation and control and simultaneously taking full advantage of surplus margin, the optimized benefit curve of the model 7 is slightly less than that of model 1 and far more than that of model 5, thus achieving mutual balance between economic benefit and control system requirements.

For possible process uncertainty, the three forms of common disturbances are considered, including sine wave, step change, and the

Table 4
Comparison with anti-interference performances of models 1 and 7.

Optimisation parameters and results	Interference function			
Process disturbance model (v)	–	$v_1 \sin\omega_1 t$	$v_2(t-t_2)$	$v_3(1-e^{-t/t_3})$
Economic benefit of the full cycle operation optimisation without margin maintaining (¥/a)	1.55×10^6	1.39×10^6	1.45×10^6	1.43×10^6
Economic benefit of the full cycle operation optimisation maintaining operation margin (¥/a)	1.49×10^6	1.42×10^6	1.46×10^6	1.45×10^6

Table 5
Comparing with anti-interference performances of model 2 and model 8.

Optimisation parameters and results	Interference function			
Process disturbance model(v)	–	$v_1 \sin\,\omega_1 t$	$v_2(t-t_2)$	$v_3(1-e^{-t/t_3})$
Economic benefit of the full cycle operation optimisation without margin maintaining (¥/a)	6.44×10^5	3.68×10^5	4.68×10^5	4.36×10^5
Economic benefit of the full cycle operation optimisation maintaining operation margin (¥/a)	5.56×10^5	4.81×10^5	5.45×10^5	5.18×10^5
Regeneration cycle of the full cycle operation optimisation without margin maintaining (day)	218.74	208.43	211.02	209.83
Regeneration cycle of the full cycle operation optimisation maintaining operation margin (day)	218.36	212.84	215.41	214.19

output of one-order inertia object, and they are added in the short time-scale dynamic optimisation model. In Table 4, v_1 and ω_1 represent the amplitude and frequency of the sine wave form disturbance; v_2 and t_2 are the amplitude and occurrence time of the step disturbance; v_3 and t_3 are the amplitude and time constant when the disturbance is in the form of a one-order inertia object.

Faced with the same disturbances, the economic benefit of the full cycle operation optimisation maintaining operation margin is more than that of the full cycle operation optimisation without margin maintaining. The full cycle operation optimisation maintaining operation margin is of superior performance for anti-disturbance.

Similar to Section 3.2, the full cycle operation optimisation model maintaining operation margin for a longer regeneration cycle solves a mixed-integer dynamic optimisation problem. Hence, based on the mixed-integer dynamic optimisation problem which can be simplified, the optimisation method in Section 3.2 is utilised for the full cycle operation optimisation maintaining operation margin. The object function of model 2 is added by the margin consumption function for realizing the full cycle operation optimisation which considers margin consumption, as shown in model 8.

Model 8

$$\min \quad J_6 = J_2 + \sum_j \delta_j^{\mathrm{R}} g_j^2(\cdot)$$

$$\text{s.t.} \quad \boldsymbol{f}(\bar{\boldsymbol{x}}, \boldsymbol{u}, \Gamma) = 0$$

$$\boldsymbol{h}(\boldsymbol{x}, \boldsymbol{u}, t) = 0$$

$$\boldsymbol{g}(\bar{\boldsymbol{x}}, \boldsymbol{u}, \Gamma) \le 0$$

$$0 < \sum_j \delta_j^{\mathrm{R}} g_j^2(\cdot) < \Delta F_1$$

The conversion factors of constraints are represented as δ_j^{R}, while the margin consumption function is represented as $\sum_j \delta_j^{\mathrm{R}} g_j^2(\cdot)$. Similar to Section 3.2, the integer variable Γ_f is treated as continuous variable to solve for the continuous dynamic optimisation problem as the form of model 8.

The optimal regeneration cycle is approximate to the model 2, and the obtained benefits are slightly less than that of model 2. In comparison with model 6, model 8 has obvious advantages in regeneration cycle and economic benefits.

Similar to Table 4, the three forms of disturbances are respectively added in the reactor model. The optimised solution of economic benefits and regeneration cycle is shown in Table 5.

Although the benefit of the full cycle operation optimisation maintaining operation margin is less than that of the full cycle operation optimisation without margin maintaining when there are no disturbances, but under the disturbance of sine wave, step change, and one-order inertia link the optimized benefit of the full cycle operation optimisation maintaining operation margin is more than that of the full cycle operation optimisation without margin maintaining. Moreover, the optimised regeneration cycle maintaining operation margin is longer than that without margin maintaining under disturbances. Comprehensively, the full cycle operation optimisation maintaining operation margin can produce optimal economic benefits and long regeneration cycle with disturbances.

5. Conclusions

Based on the established process-based model of acetylene hydrogenation reactors, this work discusses the feasibility of the full cycle operation optimisation and proposes a long time-scale dynamic optimisation model based on the estimation of operation margin. For coordinating the long time-scale dynamic optimisation and short time-scale dynamic control, the structure of double platform is used for simulation implementation with a slowly-time-varying system.

The full cycle operation optimisation of the acetylene hydrogenation reactors is solved based on CVP, and we discussed the optimal range for the number of time interval. In addition, for the full cycle operation optimisation problem, whose object is the regeneration cycle, a method is proposed to solve the continuous problem and determine the optimal solution in the feasible domain.

Based on the method of margin estimation, a full cycle operation optimisation maintaining operation margin is proposed ensuring preferable optimized results with uncertain disturbances. Although the full cycle operation optimisation without margin maintaining obtains the best effect under the ideal condition, the full cycle operation optimisation maintaining operation margin obtains the achievable better effect under disturbance condition. In comparison with the steady-state operation optimisation that ensures the design margin, the full cycle operation optimisation maintaining operation margin can obtain more economic benefits or longer regeneration cycle.

Declaration of Competing Interest

There are no conflicts of interest.

Acknowledgements

This work is supported by the National Natural Science Foundation of China (21676295).

Appendix A. Process-based model of acetylene hydrogenation based on deactivation kinetics

The kinetics equation of acetylene hydrogenation, ethylene hydrogenation and oligomer of secondary reaction product are respectively shown in Eqs. (15)–(17), respectively.

$$-r_1(Z,R,t) = k_1 \mathrm{e}^{\frac{-E_1}{\mathrm{R}gT_k^s}} p_{ck}^s(Z,R,t)\theta_k(Z,R,t) \tag{15}$$

$$-r_2(Z,R,t) = k_2 \mathrm{e}^{\frac{-E_2}{\mathrm{R}gT_k^s}} \frac{p_{bk}^s(Z,R,t)p_{ck}^s(Z,R,t)}{p_{ak}^s(Z,R,t)} \tag{16}$$

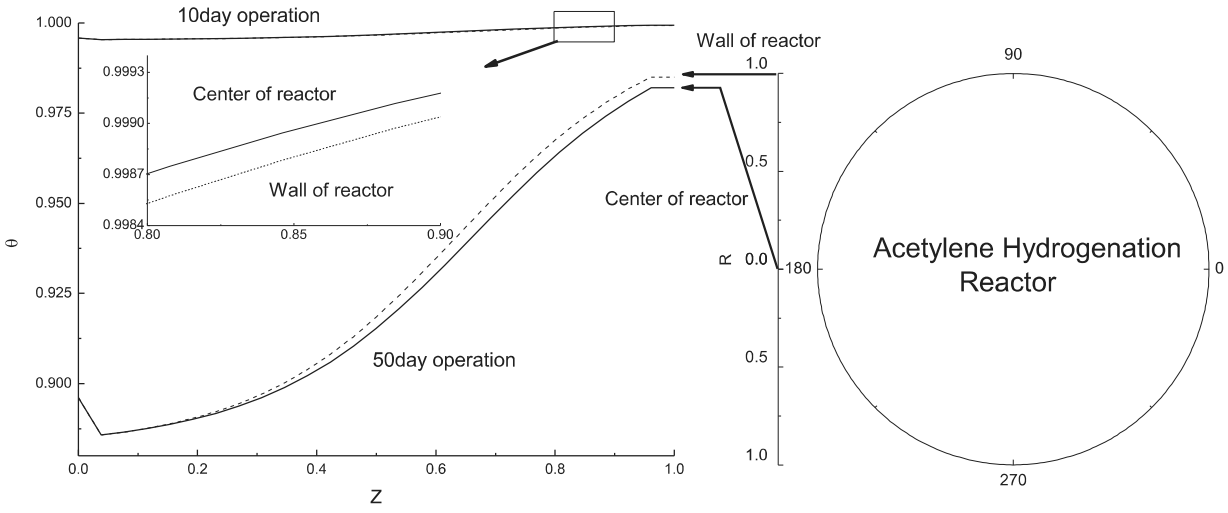

Fig. 8. Distribution of catalyst activity in the reactor.

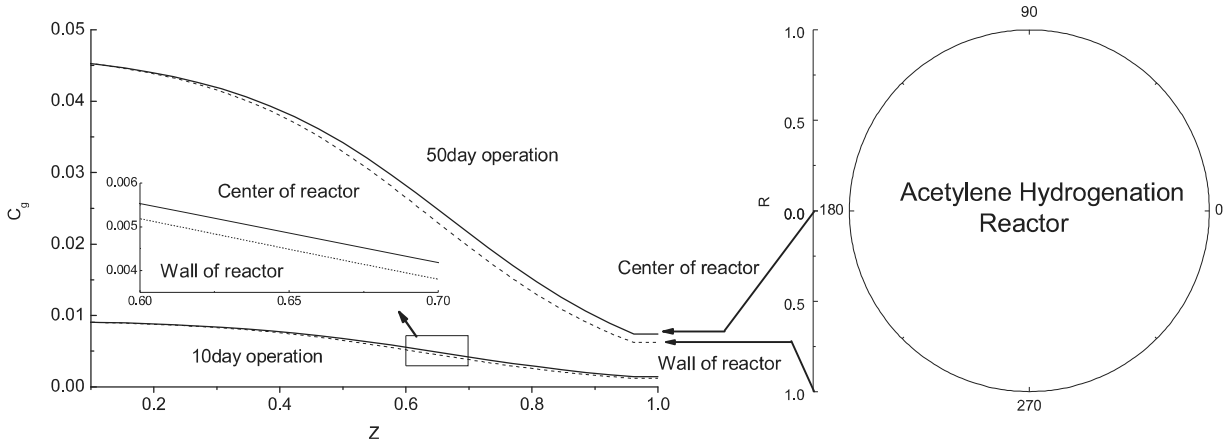

Fig. 9. Distribution of green oil concentration in the reactor.

$$-r_3(Z,R,t) = k_3 e^{\frac{E_3}{RgT_k^s}} \frac{p_{ak}^{s\,2}(Z,R,t)\,p_{ck}^{s}(Z,R,t)}{\left(1+p_{ak}^{s}(Z,R,t)\right)^3} \tag{17}$$

Generating rate of acetylene, ethylene, hydrogen and oligomer (green oil) are shown in Eqs. (18)–(21), respectively.

$$r_a = \eta_1 r_1 \tag{18}$$

$$r_b = -\eta_1 r_1 + \eta_2 r_2 \tag{19}$$

$$r_c = \eta_1 r_1 + \eta_2 r_2 \tag{20}$$

$$r_g = -r_3 \tag{21}$$

The mass balance equation for fluid phase is shown as follows:

$$\begin{aligned}\sigma \frac{\partial p_i^g k(Z,R,t)}{\partial t} &= -u\frac{\partial p_i^g k(Z,R,t)}{\partial Z} + \delta D_{Ri}\left[\frac{\partial^2 p_i^g k(Z,R,t)}{\partial R^2} + \frac{1}{R}\frac{\partial p_i^g k(Z,R,t)}{\partial R}\right] \\ &\quad + k_i^g a\left[p_i^s k(Z,R,t) - p_i^g k(Z,R,t)\right]\end{aligned} \tag{22}$$

The thermal balance equation for fluid phase is shown as follows:

$$\begin{aligned}\sigma\rho^g c_p^g \frac{\partial T_k^g(Z,R,t)}{\partial t} &= -\rho^g u c_p^g \frac{\partial T_k^g(Z,R,t)}{\partial Z} + \lambda_R^{\,g}\left[\frac{\partial^2 T_k^g(Z,R,t)}{\partial R^2} + \frac{1}{R}\frac{\partial T_k^g(Z,R,t)}{\partial R}\right] \\ &\quad + h_w a\left[T_k^s(Z,R,t) - T_k^g(Z,R,t)\right]\end{aligned} \tag{23}$$

The mass balance equation for catalyst phase is shown as follows:

$$\begin{aligned}(1-\sigma)\frac{\partial p_{ik}^s(Z,R,t)}{\partial t} &= k_i^g a\left[p_{ik}^g(Z,R,t) - p_{ik}^s(Z,R,t)\right] + (1-\sigma)\theta\, r_i\end{aligned} \tag{24}$$

The thermal balance equation for catalyst phase is shown as follows:

$$\begin{aligned}(1-\sigma)\rho^s c_p^s \frac{\partial T_k^s(Z,R,t)}{\partial t} &= h_w a\left[T_k^g(Z,R,t) - T_k^s(Z,R,t)\right] \\ &\quad + \lambda_R^s\left[\frac{\partial^2 T_k^s(Z,R,t)}{\partial R^2} + \frac{1}{R}\frac{\partial T_k^s(Z,R,t)}{\partial R}\right] + \sum_{j=1}^{2}\eta_j\theta(-r_j)(-\Delta H_j)\end{aligned} \tag{25}$$

As shown in Fig. 8, based on the heterogeneous model, the radial and axial catalyst activity in the reactor is presented on the 10th and

50th day of operation. Considering the accumulated green oil and temperature variation, the catalyst activity on the 50th day of operation is lower than that on the 10th day of operation. Considering the acetylene hydrogenation reaction depth, the catalyst activity consumption at the front of the reactor is more than the catalyst activity consumption at the end of reactor. As temperature differs between the reactor wall (radius $R = 1$) and the centre (radius $R = 0$), the radial catalyst activities have slight deviation.

Relative to activity, the radial and axial concentration of green oil is the dominant factor of long-run falling catalyst activity, as shown in Fig. 9. Oppositely, the concentration of accumulated green oil on the 50th day of operation is greater than the concentration on the 10th day of operation. Similar to the activity, as temperature differs between the reactor wall and centre, the radial rate of green oil producing slight deviates. Therefore, the radial and axial values of activity and green oil in the reactor can be accurately calculated by establishing a process-based model of catalyst activity.

Appendix B. Parameter values used in the process model

a	specific surface area of catalyst(m^{-1})	29.556
τ	number of axial discretization in the reactor	26
ω	number of radial discretization in the reactor	13
ω_1	frequency of disturbance	3
σ	catalyst porosity	0.35
η_1,η_2	efficient factor of the ethylene and ethane generated reaction	3.461, 4.26×10^{-3}
λ_R^s,λ_R^g	the catalyst and the gas phase heat conductivity coefficient of reactor radial direction ($W\ m^{-1}\ K^{-1}$)	0.578, 0.374
c_p	heat capacity ($J\ kg^{-1}\ K^{-1}$)	1.724
D_{Ra}, D_{Rb}, D_{Rc}	acetylene, ethylene and hydrogen diffusion coefficient of reactor radial ($m^2\ s^{-1}$)	2.75×10^{-5}, 3.42×10^{-5}, 7.75×10^{-6}
E_1, E_2, E_3	activation energy of reaction ethylene, ethane and green oil generated reaction ($J\ mol^{-1}$)	66.89, 52.8, 2100
E_d	activation energy of catalyst deactivation ($kJ\ kmol^{-1}$)	9.9
ΔH_1, ΔH_2	heat of the ethylene and ethane generated reaction ($J\ mol^{-1}$)	174.3,136.7
h_w	interphase heat transfer coefficient ($W\ m^{-1}\ K^{-1}$)	0.127
k_1, k_2, k_3	reaction coefficients of the ethylene, ethane and green oil generated reaction	2.64×10^3, 1.58×10^2, 2.29×10^{-2}
k_d, K_d	catalyst deactivation coefficients	6.73×10^{-3}, 3.09×10^{-3}
K_p	proportional gain of PID controller	In Fig. 2
K_I	integration time of PID controller	In Fig. 2
K_D	differentiation time of PID controller	In Fig. 2
M_a, M_b, M_c	acetylene, ethylene and hydrogen price coefficient ($RMB\ kPa^{-1}\ day^{-1}$)	2.597×10^3, 1.35×10^3, 1.685×10^2
R_g	gas constant ($J\ mol^{-1}\ K^{-1}$)	8.314
t_2, t_3	step change and one-order inertia link time constant of disturbance	200, 1.25
v_1, v_2, v_3	sine wave, step change, and one-order inertia link amplitude of disturbance	0.1, 0.05, 0.2

(*continued*)

Appendix C. Operation data of the acetylene hydrogenation reactor under normal conditions

Operating variable	Value
Hydrogen partial pressure of the first bed inlet / kPa	29.55
Temperature of the first bed inlet / K	320.8
Acetylene partial pressure of the first bed inlet / kPa	29.55
Ethylene partial pressure of the first bed inlet / kPa	1684.35
Hydrogen partial pressure of the second bed inlet / kPa	14
Temperature of the second bed inlet / K	321.8
Hydrogen partial pressure of the third bed inlet / kPa	0.79
Temperature of the third bed inlet / K	322.8

References

[1] Albers P, PietschI J, Parker SF. Poisoning and deactivation of palladium catalysts. J Mol Catal A Chem 2001;173(1):275–86.
[2] Bahri PA, Romagnoli JA, Bandoni JA, Barton GW. Back-off calculations in optimising control: a dynamic approach. Comput Chem Eng 1995;19:699–708.
[3] Binder T, Cruse A, Villar CAC, Marquardt W. Dynamic optimisation using a wavelet based adaptive control vector parameterization strategy. Comput Chem Eng 2000;24(2):1201–7.
[4] Borodzinski A, Cybulski A. The kinetic model of hydrogenation of acetylene–ethylene mixtures over palladium surface covered by carbonaceous deposits. Appl Catal A 2000;198(1):51–66.
[5] Chen TWC, Vassiliadis VS. Inequality path constraints in optimal control: a finite iteration ε-convergent scheme based on pointwise discretization. J Process Contr 2005;15(3):353–62.
[6] Chen X, Du W, Tianfield H, Qian F. Dynamic optimisation of industrial processes with nonuniform discretization-based control vector parameterization. IEEE T Autom Sci Eng 2014;11(4):1289–99.
[7] Figueroa JL, Bahri PA, Bandoni JA, Romagnoli JA. Economic impact of disturbances and uncertain parameters in chemical processes - a dynamic back-off analysis. Comput Chem Eng 1996;20(4):453–61.
[8] Galvanin F, Barolo M, Bezzo F, Macchietto S. A backoff strategy for model-based experiment design under parametric uncertainty. AIChE J 2009;56(8):2088–102.
[9] Gobbo R, Soares RP, Lansarin MA, Ferreira MP. Modeling, simulation, and optimisation of a front-end system for acetylene hydrogenation reactors. Braz J Chem Eng 2004;21(4):545–56.
[10] Hartwich A, Marquardt W. Dynamic optimization of the load change of a large-scale chemical plant by adaptive single shooting. Comput Chem Eng 2010;34(11):1873–89.
[11] Hartwich A, Schlegel M, Würth L, Marquardt W. Adaptive control vector parameterization for nonlinear model-predictive control. Int J Robust nonlin 2008;18(8):845–61.
[12] Huang W, Mccormick JR, Lobo RF, Chen JG. Selective hydrogenation of acetylene in the presence of ethylene on zeolite-supported bimetallic catalysts. J Catal 2007;246(1):40–51.
[13] Karafyllis I, Kokossis A. On a new measure for the integration of process design and control: the disturbance resiliency index. Chem Eng Sci 2002;57(5):873–86.
[14] Koller RW, Ricardez-Sandoval LA, Biegler LT. Stochastic back-off algorithm for simultaneous design, control and scheduling of multi-product systems under uncertainty. AIChE J 2018;64(13):2379–89.
[15] Kookos IK, Perkins JD. Control structure selection based on economics: generalization of the back-off methodology. AIChE J 2016;62(9):3056–64.
[16] Kuhlmann A, Bogle I. Controllability evaluation for nonminimum phase-processes with multiplicity. AIChE J 2001;47(11):2627–31.
[17] Kuhn M, Lucas M, Claus P. Precise recognition of catalyst deactivation during acetylene hydrogenation studied with the advanced Temkin reactor catalyst. Catal Commun 2015;72(2):170–3.
[18] Luo XL, Liu JX, Xu F, Zuo X. Hydrogenation, two-dimensional dynamic modeling and analysis of acetylene hydrogenation reactor. CIESC J 2008;59(6):1454–61.
[19] Luo XL, Xia CK, Sun L. Margin design, online optimisation, and control approach of a heat exchanger network with bypasses. Comput Chem Eng 2013;53(11):102–21.
[20] Mccue AJ, Mcritchie CJ, Shepherd AM, Anderson JA. Cu/Al_2O_3 catalysts modified with Pd for selective acetylene hydrogenation. J Catal 2014;319:127–35.
[21] Mehta S, Ricardez-Sandoval LA. Integration of design and control of dynamic systems under uncertainty: a new back-off approach. Ind Eng Chem Res 2016;55(2):485–98.

[22] Moayedi S, Davoudi A. Unifying distributed dynamic optimisation and control of islanded dc microgrids. IEEE T Power Electr 2017;32(3):2329–46.
[23] Morison KR, Sargent RWH. Optimisation of multistage processes described by differential-algebraic equations. Num Anal 1986:86–102.
[24] Narraway LT, Perkins JD. Selection of process control structure based on linear dynamic economics. Ind Eng Chem Res 1993;32(11):2681–92.
[25] Narraway LT, Perkins JD, Barton GW. Interaction between process design and process control: economic analysis of process dynamics. J Process Contr 1991;1:243–50.
[26] Pachulski A, Schodel R, Claus P. Kinetics and reactor modeling of a Pd-Ag/Al_2O_3 catalyst during selective hydrogenation of ethyne. Appl Catal 2012;445-446(6):107–20.
[27] Pollard GP, Sargent RWH. Off line computation of optimum controls for a plate distillation column. Automatica 1970;6(1):59–76.
[28] Rafiei-Shishavan M, Mehta S, Ricardez-Sandoval LA. Simultaneous design and control under uncertainty: a back-off approach using power series expansions. Comput Chem Eng 2017;99:66–81.
[29] Raghunathan AU, Gopal V, Subramanian D, Biegler LT, Samad T. Dynamic optimisation strategies for three-dimensional conflict resolution of multiple aircraft. J Guid Contr Dynam 2004;27(4):586–94.
[30] Rahimpour MR, Dehghani O, Gholipour MR, Yancheshmeh MS, Haghighi SS, Shariati A. A novel configuration for Pd/Ag/a-Al_2O_3 catalyst regeneration in the acetylene hydrogenation reactor of a multi feed cracker. Chem Eng J 2012;198-199:491–502.
[31] Ravanchi MT, Sahebdelfar S. Pd-Ag/Al_2O_3 catalyst: stages of deactivation in tail-end acetylene selective hydrogenation. Appl Catal, A 2016;525:197–203.
[32] Seider WD, Brengel DD, Provost AM, Widagdo S. Nonlinear analysis in process design. Why overdesign to avoid complex nonlinearities? Ind Eng Chem Res 1990;29(5):805–18.
[33] Shi J, Biegler LT, Hamdan I, Wassick JM. Optimisation of grade transitions in polyethylene solution polymerization process under uncertainty. Comput Chem Eng 2016;95:260–79.
[34] Soliman M, Swartz C, Baker R. A mixed-integer formulation for back-off under constrained predictive control. Comput Chem Eng 2008;32(10):2409–19.
[35] Srinivasan B, Palanki S, Bonvin D. Dynamic optimisation of batch processes: I. Characterization of the nominal solution. Comput Chem Eng 2003;27(1):1–26.
[36] Szukiewicz M, Kaczmarski K, Petrus R. Modeling of fixed-bed reactor: two models of industrial reactor for selective hydrogenation of acetylene. Chem Eng Sci 1998;53(1):149–55.
[37] Teo KL, Jennings LS, Lee HWJ, Renboch V. The control parameterization enhancing transform for constrained optimal control problems. J Aust Math Soc Ser B Appl Math 1999;40(3):314–35.
[38] Tian L, Jiang D, Qian F. Simulation and optimisation of acetylene converter with decreasing catalyst activity. CIESC J 2012;63(1):185–92.
[39] Tian L, Jiang D, Qian F. Reactor system switch strategy for acetylene hydrogenation process. CIESC J 2015;66(1):373–7.
[40] Tu F, Qing HY, Luo XL, Zuo X. Advanced process control of acetylene hydrogenation reactor (I): construct dynamic model. Control Instrum Chem Ind 2003;30(1):20–4.
[41] Weiss G. Modeling and control of the acetylene converter. J Process Contr 1996;6(1):7–15.
[42] Xie FM, Xu F, Liang ZS, Luo XL, Shi FY. Full-cycle operation optimisation of acetylene hydrogenation reactor. CIESC J 2018;69(3):1081–91.
[43] Xu F, Jiang HR, Wang R, Luo XL. Influence of design margin on operation optimisation and control performance of chemical processes. Chin J Chem Eng 2014;22(1):51–8.